Ultra Scientist Vol. 24(3)B, 405-410 (2012).

Studies of extended x-ray absorption fine structures of the Zinc-Beryllium-Selenide ternary solid solutions

SHABINA KHAN[a1], PANKAJA SINGH[1], JAVED MAZHER[2] and NARAYAN BEHERA[3]

(Acceptance Date 15th October, 2012)

Abstract

Hardening in the Zinc-Beryllium-Selenide ternaries has been achieved by cationic substitution alloying. Six samples of these ternaries are prepared by varying the concentration of Be dopant 'x'. EXAFS experiments for Zn core excitations are performed on the x-ray absorption spectroscopy (XAS) beamline at SOLEIL synchrotron radiation facility located at Gif sur Yvette, France. Extraction of useful EXAFS oscillations and various computational procedures require for the ZnBeSe spectral data analysis are discussed. Our analyses indicate that the hardening increases with Be-doping. Prospects of semiconductor alloy hardening through Be doping are also discussed in detail.

Key words: II-VI Mixed Alloys, Synchrotron radiation method and EXAFS.

Introduction

Group II-VI wide band gap semiconductors are suitable for both long wavelength and short wavelength optical devices like tunable blue semiconductor lasers, nano-transistors and ultra high speed and high energy switching devices[1-5]. Among these semiconductors, the zinc selenide (ZnSe) is highly suitable for deployment in the blue green lasers[6-11]. The ZnSe is a wide band gap semiconductor material and the aptness of the ZnSe mainly lies in its so called self activated emission band that is centered at 2.07 eV with the sharp lumines-cence emission lines owing to its high crystal quality and inherent strain reduction property[1,9]. However,

presence of impurities produce defects mainly from optically active centers, which largely affect any competent luminescence emission. Lasing in the ZnSe is limited because the material is not stable enough to be used in high current or in high excitation regimes[1]. Active region point defect generation and propagation are some protracted hampering issues in the zinc selenide's commercial deployment[12]. Noticeably, the ZnSe lasing devices are tricky due to ionicity induced softening of the lattice. A renewed interest in mixed ZnSe based systems arise after several recent studies[13-17] which predict large covalent bonding between dopant atoms of beryllium and chalcogenide atoms that reduces overall bond distances and brings hardening. For this reason, the $Zn_{1-x}Be_xSe$ alloys are a new class of II-VI ternary semiconducting compounds that are formed from the binaries with highly contrasting bond length-properties[15]. At this point it is highly desirable to present our the results of the extended x-ray absorption fine structure (EXAFS) measurements at Zn K edges on the compositionally varied (Zn,Be)Se alloyed samples in ambient conditions to get a better insight into the nature of Be-doping.

Experimental Techniques

Compositions of the alloy samples are varied by using the Be cationic mass fraction (x) values of 0.00, 0.06, 0.16, 0.27, 0.33, and 0.42 respectively[21]. The EXAFS experimental setup, the structural analyses routines and the investigational conditions are kept identical for all of the six samples. The XAS beamline facilitates the dispersive EXAFS that is commissioned at the SOLEIL synchrotron radiation facility located at Gif sur Yvette, France[23,24]. High synchrotron photon flux is applied and samples are positioned via piezo XY stage. A high speed CCD camera is used for detection/spectra recording in transmission mode. Focusing optics allows short acquisition time of ~2 to 12 ms [25]. A ~40μm spot size of the x-ray beam ensures a small signal to noise ratio (10^{-5}). A dipole magnet source with energy domain of ~1200 eV at 9-13 KeV range is used[26-28]. A 1.2 m long Ir and Rh bent mirror is placed just after the bending magnet source and a second mirror that is 20 cm long and placed just before the monochromator (Si-311) in Bragg geometry for rapid focus adjustment. A resolving power ($E/\Delta E$) is found to be 3×10^4 for the Si-311 and 0.7×10^4 for the Si-111. The beamline optics is also capable of adjusting the x-ray focus size of 40μm×40 μm in its full width half maxima. Finally, a computational code of ATHENA (IFEFFIT.ver.2010)[29,32] is used for the extraction of EXAFS oscillations from the x-ray absorption spectra.

Results and Discussion

EXAFS, as a local structural characterization probe, provides information on the atomic structure around its specific core atom (Zn)[30]. It gives near-neighbor atom distances and fluctuations in the bond lengths. XAS raw data is typically non-truncated and it is very difficult to extract any useful information. The ATHENA software[29] is used for spectrum truncation to obtain the correct bonding lengths from the scattering path distances in various co-ordination shells around the Zn core and its nearby atoms, this also ensures the exact chemical valance of the Zn.

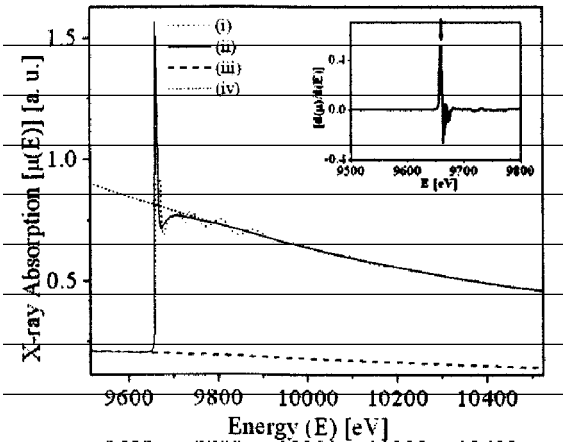

Figure 1. Zn K edge XAS for the $Zn_{1-x}Be_xSe$ sample (B) (i) Experimental data is represented by a dotted curve, (ii) Smooth continuous runner is the spline background fit, (iii) the bottom pre edge, and(iv) the top post edge. The inset is a derivative of the absorption and the maximum of the derivative, depicting the exact energy position (E_0), is indicated by the arrow mark.

The truncated spectrum shows only the oscillatory parts of the total XAS spectrum. Due to the high order of the crystallinity of the samples, only small numbers of oscillations are observable corresponding to various atomic shells around the Zn core[20-22], as shown in a figure 1. Spectral positions of these vacillations are also fairly well located with very little variations in their respective oscillatory profiles[30]. In the figure 1, a plot of the absorption coefficient is shown as a function of energy E. An overall decrease in the x-ray absorption with increasing energy is clearly noticeable. This feature is accompanied with the presence of a sharp rise in the absorption intensity at the energy corresponding to the Zn K edge that almost gives a step like absorption function (μ) at an augmentation of around 9659 eV exhibiting high rates of the optical transition and thus a high quality of the alloy crystal. At the same time, the near edge structures with an approximate width of 100 eV are also noticeable just after the edge position. We have obtained a clear series of wiggles[31] for the EXAFS oscillatory structures that clearly modulates the $Zn_{1-x}Be_xSe$ absorption pattern. This is possible owing to the high sample quality. Lastly, the step of EXAFS oscillation is concluded by subtracting the spectra from the suitable background function $m_0(E)$ above a given absorption edge, which is a smoothly varying atomic background absorption. Amid the inset of the figure 1, the top baseline that starts just after attainment of a maximum absorption is the post edge line while the bottom baseline of the absorption curve which typically covers all data points before the absorption edge represents the pre edge line. In addition, an estimate of the edge position E_0 is often made in between these onset points of pre- and post-edges[32]. However, there is no priori criterion for the E_o's determination and the problem becomes impossible to tackle when the unknown systems have constituent species of different valences and ionicities. Fortunately, in our present set of analysis the E_o is a flat parameter due to the mixed nature of the alloy. The normalization factor of the EXAFS spectra is approximated by a magnitude of the jump in the absorption at the Zn K edge that is typically of a value of 0.8 absorption units in our spectroscopic measurements. The error in this approximation can be accounted by a small (~10%) correction to the EXAFS Debye-Waller factor[34].

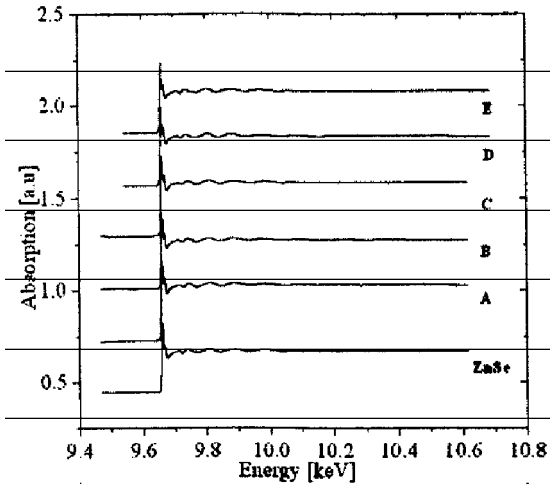

Figure 2. The normalized Zn K edge EXAFS absorption data for the $Zn_{1-x}Be_xSe$ ternary alloy samples with the composition (x) values of 0.0 (ZnSe), 0.06 (A), 0.16 (B), 0.27 (C), 0.33 (D) and 0.42 (E). The spectra are processed by using a pre edge and post edge lines and spline fitted background subtraction.

The figure 2 shows composition dependent EXAFS modulations for $Zn_{1-x}Be_xSe$ samples (A to E) in the energy range of 9500 eV to 11500 eV at 300 K. As evidenced, some weak oscillatory wiggles beyond about 30 eV above the absorption edge are obvious due to the strong scattering processes as well as local atomic resonances in the x-ray absorption, which are commonly referred to x-ray absorption near edge structure (XANES)[33]. Nevertheless, our interest is only in the fine structures that arise owing to single and multiple scatterings from atoms adjoining to the core and lying in the spectral regime of several tens of eV above the XANES region. As shown among all the spectra of the figure 2, all the modulations above the K edge are very well aligned to each other. Thus, they are undoubtedly originated from the contributions of several shells of neighboring atoms around the Zn core.

For further analysis in real-space we can effectively shield the undesired k-space oscillations by using an appropriate window. By IFEFFIT, we have converted the wide range k-space EXAFS data (k =0 to k =15 $Å^{-1}$) to real-space [$\chi(r)$] by using the fourier transforms (FTs) for the selected radial distances. Figures 3(a) & (b) represent the real and imaginary parts of these FTs. Nonetheless, a relative significance is only of the upper combined envelop these FT as shown in the figure 3(c). The enveloped function, which is also the scattering path length parameter, represents the magnitude of the FT (mag $\chi[r]$). The central maxima of the mag $\chi[r]$ show positions of the relative radial distances (scattering path lengths) in the R-space and the peak profile indicates towards possible distributions. The first peak always corresponds for first shell distances and so on[30]. We can correlate these path lengths/ distributions to bond lengths and their disorders. Although, absolute path values are found to be shifted by distances of several tenths of angstroms, a correction for these shifts is performed by using systems with known distances. Thus, we can indirectly extract the Zn-Se & Be-Se bond lengths.

The peak value of the FT-magnitude also depends on factors such as the weighting of the data, the choice of the threshold energy E, and the phase shift, which are largely responsible for the shifted FT peaks. We have obtained a constant difference between the peak in R and the neighbor distance is typically -0.45Å that is implicitly due to a scattering related phase shift [$\phi(k)$]. In the figure 3(c), the first peak

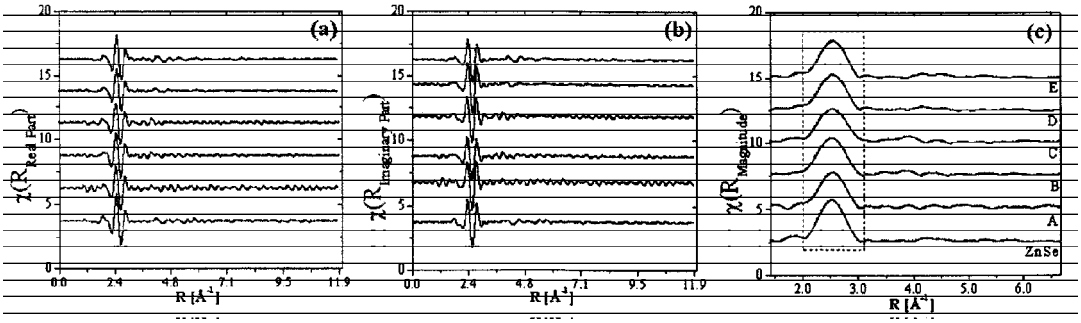

Figure 3. (a) Real-space FT plots of Zn K edge EXAFS absorption data ternary samples of $Zn_{1-x}Be_xSe$ (pure ZnSe and A-E, plotted vertically upwards), (b) Imaginary part of FTs [Im[χ (r)], (c) Magnitude profile corresponding to the function Mag[χ(r)]. A dotted box indicates the approximate position of the window for the first shell.

that is positioned at ~2.2 Å is the contribution from the first shell comprising of the four Se neighbors around the Zn core. The second peak which is observable in the figure 3(c) at the R value of ~3.4 Å is due to the contribution of the Be and Zn atoms of the second shell. We have observed a systematic displacement pattern among the second peak positions in the R-space that displaces in the range of 3.2 to 3.5 Å due to the manifestations of Zn-(Be, Se) multi bond length behaviors[18,19]. Clearly, the composition dependency of the scattering path length parameter (Mag[χ(r)]) leads to the verdict of large change in the Zn-Se bond lengths on increasing the Be content in the alloy of $Zn_{1-x}Be_xSe$ system. The as-obtained value of relative bond length change with respect to equilibrium Zn-Se bonds is found to be 0.02 Å for the alloy composition of 42% Be content $Zn_{0.58}Be_{0.42}Se$. The change indicates towards the increased solid solution hardening of the Zn-Se bonds, follows a general trend of decrease in ZnSe bonds, and thus confirms the alloy hardening. Nevertheless, on further increasing the Be concentrations, we have found decrease in the distribution (bond disorder parameter) and a minima is obtained in the sample E at 42% of Be, implying the total annihilation of alloying related multi modal bond effects. From these results we can understand that the crystal stability that is one of the main factor for preventing the solid solution hardening at the initial stages of Be-doping. However, the stability gets disturbed at higher Be concentrations and it is manifested by the reduced values of disorder. For that reason, we have obtained a clear trend of gradual increase in the solid solution hardening for alloys with Be concentrations greater than 27%.

Conclusion

The synchrotron EXAFS spectroscopy and data analyses are discussed. A comparison among the EXAFS signals are made in normalized energy-space along with extracted modulations in the R-space for better understanding of local environs of the core excitation of zinc atom in the compositionally vivid $Zn_{1-x}Be_xSe$ lattice. Significant composition dependent variations in the single scattering path length parameter have been obtained on increasing the values of the 'x' in the range of 0.06 to 0.42 and that is suitably

accredited to the alloy related hardening.

Acknowledgements

It is necessary to mention a special recognition goes to the beamline staff, synchrotron SOLEIL. They are gratefully acknowledged for their help in the EXAFS measurements under the project CEFIPRA-3204-1.

References

1. Pawlis A., Panfilova M., Sanaka K., Phys. Rev. B 84, 115201 (2011).
2. Lach P., Karczewski G., Wojnar P., J. of Luminescence, 132, 1501 (2012).
3. Huang C.W., Weng H.M., Jiang Y.L., Vacuum, 83, 313 (2009).
4. Nanavati S.P., Sundararajan V., Mahamuni S., Phys. Rev. B, 80, 245417 (2009).
5. Toda A., Nakamura F., Yanashima K., J. of Crystal Growth, 170, 461 (1997).
6. Kasai J.I., Akimoto R., Hasama T., *Appl. Phys. Expr. 4,* 082102 (2011).
7. Haase M/.A., Qiu J., DePuydt J.M., *Appl Phys Lett, 59,* 1272 (1991).
8. Ahmed M.U., Irvine S.J.C., Stafford A., J. of Crystal Growth, 180, 167 (1997).
9. Takahashi T., Nakamura T., and Adachi S., Opt. Lett. 34, 3923 (2009).
10. Nomura I., Sawafuji Y., and Kishino K., Jpn. J. Appl. Phys. 50, 031201 (2011).
11. Worschech L., Ossau W., Lugauer H.J., J. of Crystal Growth, 184, 500 (1998).
12. Verie C., J. Crystal Growth 184, 1061 (1998).
13. Maksimov O., Rev. Adv. Mater. Sci. 9, 178, (2005).
14. Berghout A., Zaoui A., Hugel J., Phys. Rev. B 75, 205112 (2007).
15. Dumcenco D.O., Huang C.T., Huang Y.S., Phys. Rev. B 79, 235209 (2009).
16. Lugauer H.J., Keim M., Reuscher G., J. Cryst. Growth 201, 927 (1999).
17. Plazaola F., Flyktman J., Saarinen K., J. of Appl. Phys. 94, 1647 (2003).
18. Ganguli T., Mazher J., Polian A., J. Appl. Phys. 108, 083539 (2010).
19. Zakrzewski J., Malinski M., Phys. Stat. Sol. (C) 3, 746 (2006).
20. Bukaluk A., Wronkowska A.A., Wronkowski *A., Appl. Surface Sc. 175,* 531 (2001).
21. Malinski M., Chrobak L., Zakrzewski J., Opto-Electronics Review 19, 183 (2011).
22. ODE beamline (2007) URL: www.synchrotron-soleil.fr/Recherche/LignesLumiere/ODE
23. Baudelet F., Kong Q., Nataf L., J. High Pressure Research 31, 136 (2011).
24. Dartyge E., Depautex C., Dubuisson J.M., Nuclr Instr. and Met in Phys Res Sec A 246, 452 (1986).
25. Matsuchita T., Phizackerley R.P., *Jpn. J. Appl. Phys. 20,* 2223 (1981).
26. Pimpale A.V., Nandedkar R.V., Synchrotron Radiation News 16, 17 (2003).
27. Newton M.A., Beek W.N., Chem. Soc. Rev. 39, 4845 (2010).
28. Bhattacharyya D., Poswal A.K., Nuclr Instr. and Meth in Phys Res Sect A 609, 286 (2009).
29. Ravel B., Newville M., J. of Synchrotron Radiation 12, 537 (2005).
30. Lee P.A., Citrin P.H., Eisenberger P., Rev. Mod. Phys. 53, 769 (1981).
31. Sayers DE, Bunker B, "X-Ray Absorption", Wiley, New York, pp 216 (1988).
32. IFEFFIT Documentation (2010) URL: http://cars9.uchicago.edu/ifeffit
33. Rehr J.J., Albers R.C., Natoli C.R., Phys. Rev. B 34, 4350 (1986).
34. Babanov Y.A., Shvetsov V.R., Phys Stat Sol B 131, 1 (1985).